Journal of The Electrochemical Society, 2023 **170** 014505

Anolyte Enhances Catalyst Utilization and Ion Transport Inside a CO_2 Electrolyzer Cathode

Prantik Saha,[*] Danielle Henckel, Fry Intia, Leiming Hu, Tim Van Cleve,[z] and K. C. Neyerlin[z,*]

Chemistry & Nanoscience Center, National Renewable Energy Laboratory, Golden, Colorado, United States of America

Electrochemical CO_2 reduction is a promising technology to capture and convert CO_2 to valuable chemicals. High Faradaic efficiencies of CO_2 reduction products are achieved with zero-gap alkaline CO_2 electrolyzers with a supporting electrolyte at the anode (anolyte). Herein, we investigate the effect of anolyte on the electrode properties such as catalyst utilization, ionic accessibility etc. of a CO_2 reduction cathode using electrochemical techniques and cell configurations that avoid the complexities related to co-electrolysis. Using 1M KOH as the anolyte and a Cu gas-diffusion-electrode with low Nafion content as the model CO_2 reduction electrode, we find that electrode capacitance (proxy for electrochemically active surface area) and ionic conductivity inside the cathode increase approximately 4 and 447 times, respectively, in presence of KOH. Liquid anolyte wets the electrode's pore structure more efficiently than capillary condensation of feed water vapor. The ionomer coverage is very low, and its distribution inside the electrode is highly fragmented. Surface ion conduction mechanisms inside the electrode are orders of magnitude lower than the bulk ion conduction in presence of anolyte. This study shows that when an anolyte (e.g., KOH) is used, catalyst utilization and ionic accessibility inside the electrode increase significantly.

 [DOI: 10.1149/1945-7111/acb01d]

Manuscript submitted August 5, 2022; revised manuscript received December 9, 2022. Published January 26, 2023.

Supplementary material for this article is available online

Despite significant progress in the commercialization of carbon-neutral technologies, global carbon emissions has remained significant. In 2019, it was approximately 5.42 GtC/yr, with an average of 5.07 ± 0.76 GtC/yr during the last 10 years[1]. To compensate these huge emissions and keep the Earth's temperature below the 1.5° C limit recommended by the 2015 Paris Accord, CO_2 capture, conversion or sequestration is essential. Among different carbon capture and utilization technologies, electrochemical CO_2-reduction (CO_2R) is a promising approach. It can efficiently capture CO_2 from the effluent gases of heavy industries (e.g., fossil-fuel power plants, steel, cement factories etc.) and convert it to valuable chemicals like CO, C_2H_4, C_2H_5OH, HCOOH, etc. Historically, CO_2 reduction reactions (CO_2RR) were limited to low current densities[2] due to the low solubility and diffusivity of CO_2 in liquid electrolytes.[3] High current densities and Faradaic efficiencies of CO_2RR products were achieved using gas diffusion electrodes (GDE) with zero-gap cell configurations (no electrolyte layers separating electrodes from the membrane).[4] This was an improvement over cell designs with flowing catholyte where high ohmic resistances limited the energy efficiency for such devices.

A typical zero-gap CO_2 reduction cell consists of three parts- CO_2 reduction cathode, a polymeric ion conduction membrane, and a water electrolysis anode. During CO_2 electrolysis, the potential at the cathode is negative with respect to the reversible hydrogen electrode (RHE), so, both CO_2RR and hydrogen evolution reaction (HER) occur at that potential. Anion exchange membranes (AEM) are typically used to facilitate CO_2RR over HER. Often, an anolyte (KOH or $KHCO_3$) is circulated to improve the water-splitting kinetics at anode and ionic conductivity of the membrane,[5] and maintain an alkaline environment at the cathode to facilitate CO_2RR over HER.[6,7] In literature, some studies focused on the enhancement of CO_2RR kinetics by the anolyte. But there is no electrode-level studies that clearly analyzes the impact of the flowing anolyte on the catalyst utilization and ionic accessibility inside the cathode catalyst layer. The electrode properties include, but not limited to, catalyst utilization and ionic conductivity inside the electrode.

CO_2RR is strongly dependent on the local reaction environment[8] at the catalyst-electrolyte interface like pH,[9] concentration of the supporting electrolytes,[10] type of cations in the supporting electrolyte[11] etc. Moreover, different catalyst-electrolyte interfaces (e.g., catalyst-water, catalyst-electrolyte, catalyst-ionomer) co-exist within the cathode. As water acts as the proton donor for CO_2RR in alkaline environment,[2] it can originate from both the anolyte and capillary condensation of the feed water vapor used to humidify CO_2. Previous studies indicate that anolyte provides the water responsible for CO_2RR during dry CO_2 feed.[12] Moreover, it was also found that the CO_2RR performance does not depend strongly on the level of CO_2 humidification as long as an optimum level of anolyte circulation is maintained. However, if the feed gas is completely dry, carbonate and bicarbonate salts precipitate from the reaction of CO_2 and OH^- resulting in higher Ohmic resistance in the cell.[12] This indicates that during CO_2RR in presence of an anolyte, the reaction dominantly occurs at the catalyst-anolyte solution interface. In addition, CO_2RR performance also depends on the catalyst-ionomer interactions, possibly due to catalyst utilization, stabilization of the reaction intermediates, and hydrophilicity of the ionomer side chain.[13–15] However, it is not clear if the dependence of CO_2RR on the ionomer binder is an effect related to the overall electrode properties like catalyst utilization, or improved reaction kinetics (e.g., stabilization of the reaction intermediates). Nafion is often used as the cathode catalyst layer binder material for its chemical stability and water sorption abilities, even though it does not conduct anions. It may also make the local catalyst environment more alkaline and facilitates CO_2RR over HER,[8] but precisely how much of the catalyst active area is covered by ionomer has never been assessed.

These observations motivated us to design a study that can systematically investigate the following issues- 1) the effect of anolyte on catalyst utilization in the cathode, 2) ionic conductivity inside the electrode with and without anolyte, 3) ionomer coverage on the catalyst particles, and 4) estimated catalyst area interacting with the anolyte solution. As we focused solely on the morphological aspects of the cathode, we did not use any CO_2 electrolyzer setup. Instead, we used an anode that consisted of Pt supported on C, a membrane, and a Cu GDE with low Nafion content as the model CO_2RR electrode. Cu catalysts show good Faradaic efficiencies for

*Electrochemical Society Member.
[z]E-mail: Timothy.VanCleve@nrel.gov; Kenneth.Neyerlin@nrel.gov

C_2 products.[6,9,16] 1 M KOH was chosen as the anolyte. Comparing the catalyst utilization and ionic conductivity data in presence and absence of anolyte, we examine the role of anolyte on the cathode properties. Based on these results, we also comment on the limitations of building a CO_2 electrolyzer without any flowing anolyte. The novelty of this study lies in the cell and experimental design that enabled us to focus on the cathode's morphological aspects without any complexities of water electrolysis (oxygen evolution reaction or OER) at the anode.

The capacitance, ionic conductivity, ionomer coverage data etc. obtained for a CO_2RR electrode using this method can be used to explain its overall performance (Faradaic efficiency, overpotential etc.) in a practical CO_2 electrolyzer. However, it requires detailed modeling of water splitting reaction in the anode, ion conduction and product crossover through the membrane, and CO_2 reduction kinetics by systematically considering local pH and CO_2 concentration. The complexity of such an analysis is beyond the scope of this work. Instead, we focus on analyzing the effect of anolyte on CO_2RR electrode properties (catalyst utilization, ionic conductivity etc.) in this study. It has to be kept in mind that the numerical values of capacitance, ionic conductivity inside the electrode can depend strongly on the type of anolyte (e.g., KOH or $KHCO_3$) as well as its concentration. So, the results of this analysis should be interpreted qualitatively, i.e., as generic effects of anolyte on CO_2RR electrode properties. In future, this electrode characterization technique will be used to explain the performance of a real CO_2 electrolyzer, and to systematically design efficient electrodes with high catalyst utilization and ionic conductivity.

Methodology and Cell Configurations

As mentioned in the previous section, we used a Cu GDE with low Nafion content (details in the Experimental section) as the model CO_2RR electrode in this study because of its high FE toward C_2 products.[8,9,14,17,18] To understand the role of anolyte (KOH in this study) on the CO_2RR electrode, we measured the catalyst utilization, catalyst-ionomer interactions, and ionic conductivities inside the electrode using different cell configurations summarized in Fig. 1. Catalyst utilization was measured using electrode capacitance. EIS was used as the main experimental tool to calculate capacitance and ion-transport resistances. We fed the Pt/C anode with H_2 and the Cu GDE with N_2 gases. H_2 at Pt enabled us to control the potential on the cathode with precision and provided a good reference electrode. It was also the counter electrode. By using a Pt reference/counter electrode, we also avoided the complexities of OER that occurs in a practical CO_2 electrolyzer. Using N_2 at the cathode, we avoided the complexities of Faradaic reactions to a great extent. In practical conditions, Faradaic reactions like oxide formation on Cu and oxidation of H_2 that crosses over the membrane do occur and are accounted for in the data analysis.

The effect of anolyte KOH on the cathode properties (catalyst utilization, ionic accessibility etc.) was determined in the following way- first, we measured the capacitance and ion-transport resistance of the electrode without any anolyte. Both cation-exchange-membranes (CEM) and AEMs were used. The configurations with a CEM and an AEM are shown in Figs. 1a and 1b respectively. Then, we repeat the experiments with the same AEM but in presence of flowing KOH as depicted in Fig. 1c. To avoid flooding in the anode and ensure adequate H_2 accessibility, the anolyte chamber was separated from the Pt/C electrode by another membrane of the same kind. Comparing these properties in presence and absence of KOH, we determine the role of KOH on the Cu GDE. These setups avoid the OER-related complexities of a CO_2 electrolyzer and elucidates the properties of the CO_2R cathode in the simplest possible way.

We also explain how these different experimental conditions (Figs. 1a–1c) reveal different electrochemical interfaces and ion-conduction mechanisms inside the Cu GDE. They are shown in the relevant zoomed-in boxes (Figs. 1a–1c). When a CO_2 electrolyzer operates, different electrochemical interfaces and ion-transport mechanisms become active inside a CO_2RR GDE. The experimental setups in Figs. 1a–1c help to determine them. Table I describes the major and minor active interfaces and ion-conduction mechanisms for different cell configurations in Fig. 1. Detail of the setup and experimental procedure are provided in the Experimental section.

In the CEM cell configuration (Fig. 1a), H^+ conduction occurs inside the electrode through the Nafion chains as well as through water confined inside the pores. Although ionic conductivity is very low in bulk water, it is several orders higher in magnitude for confined water.[19,20] The latter is often called surface conduction of ions where the term "surface" refers to the local catalyst particle-water interface. This phenomenon has been studied from fundamental electric double layer perspective[21–23] as well as in porous

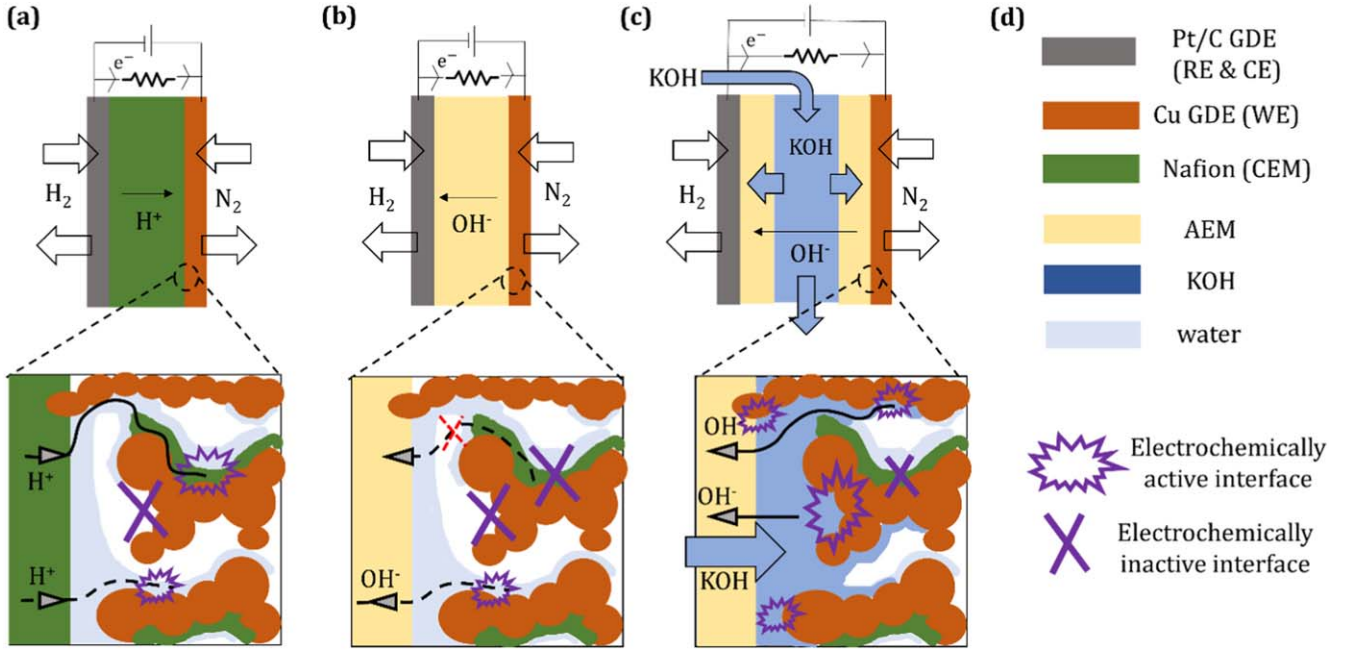

Figure 1. Schematic of the experimental setups: (a) MEA with a CEM without KOH flow, (b) MEA with an AEM without KOH flow, and (c) with AEMs and KOH flow, (d) legends. The explosion and the cross symbols show the electrochemically active and inactive interfaces respectively.

Table I. Active interfaces and ion-transport mechanisms for different setups in Fig. 1.

Setup label	Setup details	Electrochemically active interfaces		Ion-conduction mechanisms	
		Major	Minor	Dominant	Secondary
a)	Cu GDE with CEM, no anolyte (KOH) flowing	Cu-H_2O	Cu-Nafion	H^+ conduction via Nafion	Surface conduction of H^+ ions
b)	Cu GDE with AEM, no anolyte (KOH) flowing	Cu-H_2O	Cu-Nafion	Surface conduction of OH^- ions	H^+ conduction via Nafion
c)	Cu GDE with AEM and anolyte (KOH) flowing	Cu-KOH	1. Cu-Nafion 2. Cu-H_2O	Bulk ion-conduction through KOH	1. H^+ and K^+ ion conduction through Nafion 2. Surface ion conduction

electrodes.[24–26] From the impedance measurements at low and high relative humidity (RH) of the cathode gas feed, we calculate- 1) the ionomer coverage, and 2) H^+ conductivity inside the electrode. The ionomer coverage is calculated by comparing the electrode capacitance at very low and high RH.[27] The following equations apply for this setup:

$$C(RH)|_{CEM} = C|_{Cu-Nafion} + C(RH)|_{Cu-H_2O} \quad [1]$$

$$\kappa(RH)|_{CEM} = \kappa(RH)|_{H^+,\,Nafion} + \kappa(RH)|_{H^+,Cu-H_2O} \quad [2]$$

In Eq. 1, $C(RH)|_{CEM}$ refers to the total capacitance measured with a CEM at any given RH. $C|_{Cu-Nafion}$ and $C(RH)|_{Cu-H_2O}$ are the capacitances from the Cu-Nafion and Cu-water interfaces respectively. We assumed that the capacitance at the Cu-Nafion interface does not strongly depend on RH because of low Nafion loading in these Cu electrodes. The term Cu-H_2O refers to the Cu-water interface where water is formed due to capillary condensation of the vapor used to humidify the cathode feed. In Eq. 2, $\kappa(RH)|_{CEM}$ is the overall ionic conductivity through the electrode at any given RH. $\kappa(RH)|_{H^+,Nafion}$ is the ionic conductivity of H^+ though the Nafion chains and $\kappa(RH)|_{H^+,Cu-H_2O}$ is the surface conduction of H^+. The total H^+ conductivity is the sum of H^+ conductivities occurring via these parallel channels.

In the second cell set-up (Fig. 1b), we assembled the MEA with an AEM without any flowing anolyte. In this configuration, OH^- conduction in the electrode predominantly occurs at the Cu-H_2O interface as the bulk ionic conductivity of water is very low, and Nafion transports cations (e.g., H + or K+). For the AEM case, we have:

$$C(RH)|_{AEM} = C|_{Cu-Nafion} + C(RH)|_{Cu-H_2O} \quad [3]$$

$$\kappa(RH)|_{AEM} \approx \kappa(RH)|_{OH^-,Cu-H_2O} \quad [4]$$

Equations 1 and 3 are approximately equal, as capacitance comes from the electroactive area of the catalyst layer irrespective of the conducting ions. Equation 4 only assumes the dominant ion-conduction mechanism, i.e., OH^- conduction over the Cu surface. In principle, Nafion chains can also conduct H^+, but in this case, a bipolar-junction would appear inside the electrode as it is in contact with an AEM. The water splitting reaction has to occur at the water-Nafion junction. The data (Fig. 4) shows that its effect is much smaller in magnitude than the dominant mechanism, so, its contribution is negligible.

After investigating the Cu electrode properties without KOH in the first two cell configurations, the electrolyte was introduced in the third step (Fig. 1c). In this set-up, KOH was flowed in a chamber created between the anode and the cathode (details in the Experimental section). The KOH chamber was kept separated from both electrodes by two AEMs. KOH crossed through the AEM to penetrate inside the Cu GDE. This mimics the situation in a practical CO_2 electrolyzer where KOH fed as the anolyte crosses over to the cathode through the anode and the membrane. The KOH crossover rate is strongly dependent on the properties of the specific AEM and is not universal. We have the following relations:

$$C(RH)|_{AEM+KOH} = C|_{Cu-Nafion} + C(RH)|_{Cu-H_2O} + C|_{Cu-KOH} \quad [5]$$

$$\kappa(RH)|_{AEM+KOH} \approx \kappa(RH)|_{K^+,Nafion} + \kappa(RH)|_{OH^-,Cu-H_2O} + \kappa|_{KOH} \quad [6]$$

In Eq. 5 the term $C|_{Cu-KOH}$ refers to the Cu-KOH solution interface. This is the extra interface in presence of KOH. Similarly, in Eq. 6, $\kappa|_{KOH}$ refers to the conductivity through the KOH phase inside the electrode. Both these quantities are RH independent as they are liquid in nature. The conductivity with KOH flow can be assumed to be bulk ionic conductivity and both K^+ and OH^- contribute to the process. $\kappa(RH)|_{K^+,\,Nafion}$ is the conduction of K^+ through Nafion chains. It is important to note that in presence of KOH solution, Nafion chains can conduct both H^+ and K^+. As this setup has an AEM, the amount of H^+ present in the electrode is significantly less than that with a CEM (Fig. 1a). Therefore, the ionic conductivity of Nafion within the Cu electrode will primarily result from K^+ conduction.

An additional electrode set-up was used, where there was no flowing KOH, but the electrode was pre-soaked in KOH before being assembled in the cell. KOH stuck to the electrode, bridged the microscopic gap between the membrane and the GDE, and reduced the overall Ohmic resistance of the cell. When we compare the results of this setup with that from Fig. 1c, we can determine the effect of KOH cross-over through the membrane and penetration inside the GDE.

Next, we explain how capillary condensation effect can be used to determine the electroactive catalyst area. If water vapor is mixed with the feed gas (H_2 or N_2), upon entering the electrode, it will condense to form water inside those pores whose size are less than a certain radius (r_{pore}) determined by the Ostwald-Freundlich equation, a variation of the Kelvin equation.[28] For low RH, vapor condenses to

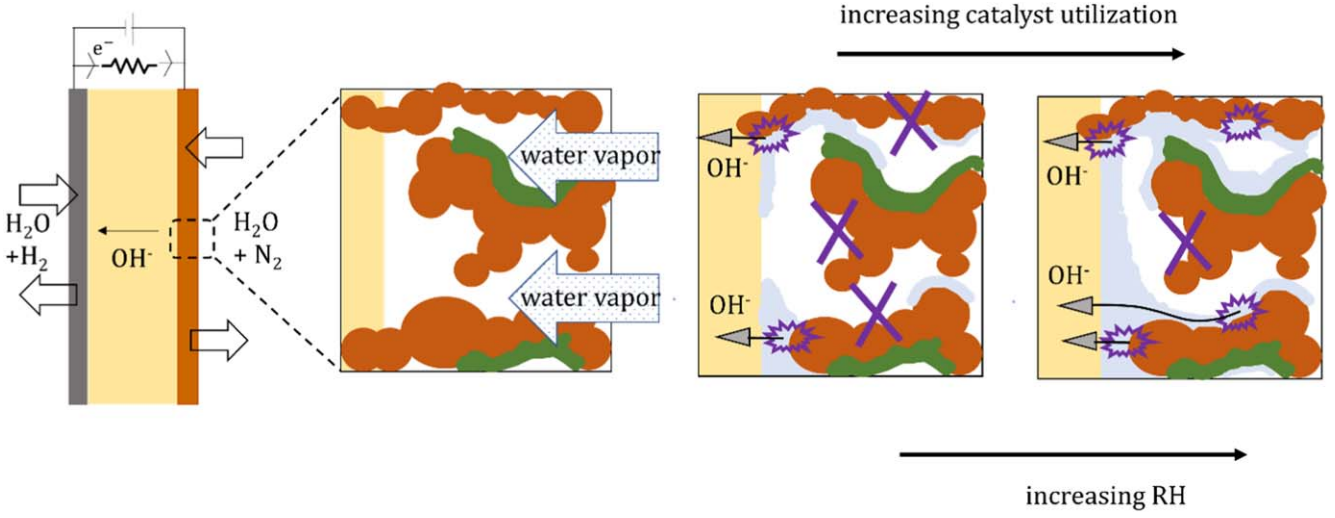

Figure 2. Schematic of how capillary condensation of vapor makes more catalyst area electrochemically active. When RH is low, condensation occurs inside the smaller pores first. With increasing RH, water fills up larger pores. Capacitance and ionic conductivity increase with increasing RH.

form water inside smaller pores. When RH is increased, vapor condenses into larger pores. The pores that have liquid water inside them may become electrochemically active, as ion conduction (H^+ and OH^-) can occur in those domains. With increasing RH, more pores become electrochemically active. Experimentally, this implies that capacitance and ionic conductivity will increase with RH. This is explained schematically in Fig. 2:

This phenomenon is also important from another reason. As mentioned before, water acts as the source of protons for both CO_2RR and HER in alkaline environment. In a CO_2 electrolyzer cell, there are two possible sources of water- 1) the anolyte KOH solution, and 2) water formed by capillary condensation from the feed vapor. Experimental evidence suggest that the anolyte KOH solution is the principal source of water.[12] By comparing the experimental results with and without KOH, this will be verified later.

As mentioned earlier, EIS was performed to measure the capacitance and ionic conductivity of the Cu GDE. The data were fitted with a transmission-line model.[29–31] The overall measured impedance takes the form:

$$Z_{net} = Z_{membrane} + Z_{cathode} + Z_{DM} \approx R_\Omega + j\omega L + \sqrt{R_{CL} Z_{int}} \times coth\left(\sqrt{\frac{R_{CL}}{Z_{int}}}\right) \quad [7]$$

The impedance from the anode can be assumed to be 0 (SM S1). In Eq. 7, R_Ω is the Ohmic resistance (also called high-frequency resistance or HFR) which is the sum of the ion-conduction resistance through the membrane (H^+ in case of CEM, and OH^- for AEM) and electronic resistance through the catalyst layer, the diffusion media (abbreviated as DM), the flow fields, and the current collectors. The contribution of the electronic resistance is usually insignificant[30] unless a significant surface oxidation occurs on the DM or flow fields. In our setup, humidified H_2 is fed at the anode. As a result, the surface oxide effect on electronic conductivity can be neglected. In a practical CO_2 electrolyzer, the electronic resistance could be high due to oxide formation on the anode flow field and the diffusion medium. R_Ω is not particularly relevant to understand the cathode properties such as catalyst utilization and ionic accessibility. So, we reported their values in SM S2. Z_{int} denotes the interfacial resistance ($Z_{int} = R_{CT}/[1 + j\omega C R_{CT}]$) at the catalyst-electrolyte interface inside the electrode. C denotes the electrode (sheet) capacitance of the cathode and R_{CT} is the Faradaic charge transfer resistance. For unsupported catalyst (as in this study), the capacitance acts as a good measure as the active catalyst area. All EIS experiments were performed at the same potential (100 mV DC and 20 mV AC root mean square). R_{CL} is the ion-transport resistance (H^+ in case of CEM, and primarily OH^- for AEM and KOH) inside the cathode as known as the electrode sheet resistance. "j" is the imaginary number ($\sqrt{-1}$). $\omega = 2\pi\nu$, where ν is the angular frequency of the oscillation (measured in Hz). L is the inductance (from all the metallic parts in the circuit). Data analysis techniques are discussed in the SM S1 and S2.

Results and Discussion

EIS experiments were performed with all configurations shown in Figs. 1a–1c. First, we show how the capacitance changed with RH with and without KOH in Figure 3–3(a) shows the plot of capacitance vs RH, and 3(b) shows schematic of active interfaces for different settings.

Data in Fig. 3 show that for both AEM and CEM, the capacitance increases with RH. N_2 was fed at cathode to ensure that the electrode charging is dominantly capacitive. However, Faradaic reactions still occur due to the presence of water and oxidation of the H_2 that crosses through the membrane. For this study, Faradaic charge transfer resistance values are not directly relevant. But we reported them in SM S2 for the sake of completeness. At very low RH, the electrode does not have much condensed vapor and catalyst-ionomer interface was the active electrochemical interface. This is the reason why capacitance values at low RH were very similar for both AEM and CEM since similar Cu electrodes were used in these two cell configurations. In the intermediate RH range, capacitance was higher for CEM than AEM. Hydration number (λ) represents the number of water molecules per functional group in the membrane and is a good measure of a its water uptake capability. λ of Nafion XL is higher than Hexamethyl-p-terphenyl poly(benzimidazolium) membrane. The first one was used as the CEM and the latter as the AEM (25 μm thick Aemion+, Experimental section). For example, at 60% RH, the λ for the CEM is close to 8,[32] whereas for the AEM, it is close to 4[33] at similar temperature. Hence, the CEM was better at absorbing water than the AEM. Actual water content in the electrode varies depending on the water-sorption properties of the membrane. Because of this reason, the electrode with CEM had more water than that with the AEM in the intermediate RH range. Hence, the electrode capacitance was higher. At very high RH, the capacitance values for both CEM and AEM converge to a similar value (hydration number close to 12 for both membranes[32,33]). This is the maximum catalyst utilization that can be achieved by capillary condensation of the feed water vapor for the membranes used (Nafion XL as the CEM and reinforced Aemion + as the AEM). In general, this maximum value of capacitance could be different with different membranes. The ionomer coverage can be calculated, both for CEM and AEM, by taking the high and low RH limits of Eqs. (1) or (3) as (Table II):

In both configurations, ca. 4% of the catalyst active area is covered by ionomer (Nafion). The similarity of the electrode capacitances suggests minimal electrode variability using this specific electrode fabrication method (Experimental).

We also repeated the experiment at 100% RH with an electrode that was presoaked in 1 M KOH solution. Cell ohmic resistance with GDE is typically higher than catalyst-coated membranes (CCM) due to the lack of strong contact between the membrane and the electrode.[34] This makes ion-conduction between the GDE and the membrane less efficient. When the MEA was assembled with the wet GDE, the KOH film acted as ion-bridge between them. This decreased the overall ohmic resistance of the cell (SM S2) and improved the catalyst utilization by penetrating inside the GDE due to the capillary effect.

Next, we describe the physical significance of the measured capacitance values when KOH was flowing (Fig. 1c). During this experiment, the electrode was not pre-soaked with KOH. So, it did not have any KOH initially. Any KOH that entered the GDE must have crossed over through the AEM separating it from the KOH chamber, mimicking the actual situation in a CO_2 electrolyzer. The measured capacitance was 5064.52 μF cm^{-2} for dry N_2 feed and 5702.69 μF cm^{-2} for 95% RH gas feed. These values were corrected for the capacitance of a bare GDL with flowing KOH (SM S2). The capacitance increased only by 12.6% for 95% increase in RH. This result is of tremendous importance. It implies that when KOH is flowing, catalyst utilization is much higher than the case when it is

Table II. Ionomer coverage for Cu.

Membrane	C(RH = 20) (μF/cm2)	C(RH = 100) (μF/cm2)	Ionomer coverage
CEM (Nafion XL)	55.24	1475.76	3.74%
AEM (Ionomr)	57.45	1350	4.26%

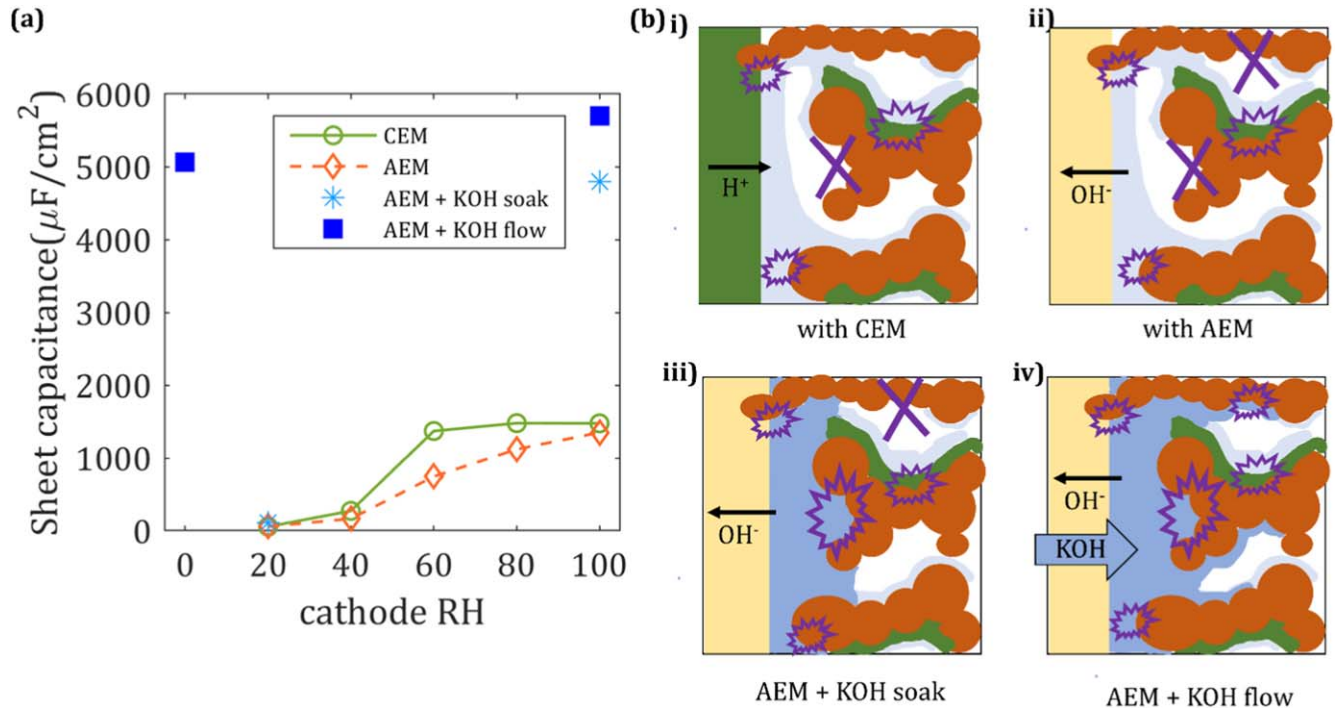

Figure 3. Cathode capacitance vs RH curve shows the catalyst utilization in different experimental conditions. With KOH flow, the utilization was much higher.

not flowing. Secondly, with flowing KOH, the feed RH does not contribute appreciably to catalyst utilization. Using Eq. 5, we can put $C(RH = 100)|_{AEM+KOH} = 5702.69\ \mu F\ cm^{-2}$. Also, at 0% RH, $C|_{Cu-H_2O} = 0$. So, $C|_{Cu-KOH} = C(RH = 0)|_{AEM+KOH} - C|_{Cu-Nafion}$ = (5064.52–57.45) $\mu F\ cm^{-2} = 5007.07\ \mu F\ cm^{-2}$. (Table I, AEM). Like ionomer-coverage, one can also calculate the portion of catalyst active area covered by KOH solution, using Eq. 5 to be:

$$KOH\ coverage = \frac{C|_{Cu-KOH}}{C(RH = 100)|_{AEM+KOH}} \frac{5007.07\ \mu F/cm^2}{5702.69\ \mu F/cm^2} \times 100 = 87.8\%$$

Using Eq. 5 and data in Fig. 3, we can tabulate the relative abundance of different interfaces inside the CO_2R electrode (with AEM membrane) in the following Table III:

This result strongly indicates that Cu-KOH interface is the most dominant for Faradaic reactions (both CO_2RR and HER). Similar results were also found for the anode of an alkaline electrolyzer.[5] This also indicates that the liquid KOH wets the pore-space inside the electrode better than capillary condensation. Another important comparison can be done between the capacitance values during KOH soak and KOH flow. During KOH soak, the capacitance was 4657.13 $\mu F\ cm^{-2}$ (corrected for a bare GDL, SM S2), which is 81.66% of the capacitance measured during KOH flow. This indicates that during soak, the KOH solution penetrated the Cu GDE significantly due to the capillary action. The calculation in Table III neglects the difference in dielectric properties of these interfaces, i.e., Cu-Nafion, Cu-H_2O, and Cu-KOH. A more refined calculation, albeit with more physical approximations, is presented in SM S3. The results, however, do not change by more than a few percentages.

Now, we present the ionic conductivity inside the electrode vs RH data for different experimental conditions in Figs. 4–4a shows the numerical values, 4b shows the ion-conduction mechanisms for different experimental setups, and 4c shows the legends. The *Y*-axis (electrode conductivity) is plotted in logarithmic scale as it strongly depended on the feed RH, when no KOH was present. This conductivity trend with hydration is also well-known for Nafion membranes.[35] From the EIS data, area specific sheet resistance was calculated by fitting it with the high-frequency limit of the transmission-line model (SM S1 and S2). Then, conductivity was calculated with the knowledge of electrode thickness. The thickness was measured by micro-XCT (Experimental and SM S5).

In Fig. 4a, the sheet conductivity increased with increasing RH. For CEM setup (Fig. 1a), the sheet conductivity increased from $\sim 1.04 \times 10^{-6}$ S cm^{-1} at 20% RH to $\sim 4.39 \times 10^{-4}$ S cm^{-1} at 100% RH. For the AEM setup (Fig. 1b), the sheet conductivity was much lower, but increased similarly from $\sim 1.79 \times 10^{-9}$ S cm^{-1} at 20% RH to $\sim 4.54 \times 10^{-7}$ S cm^{-1} at 100% RH. Ionic conductivity in AEM configuration was orders of magnitude lower, for any given RH, because of the difference in ion-conduction mechanism. In the CEM configuration, H^+ conduction can occur both via Nafion chains and along the Cu surface (covered by water). So, even when the RH was low, Nafion chains could still conduct H^+, although the cationic conductivity of Nafion was less for reduced RH. The situation is depicted in Fig. 4ai. In the case of AEM (Fig. 4bii), the only available mechanism for OH^- conduction was along the Cu surface.

Table III. Relative abundance of different interfaces.

Interface	Mathematical symbol used	Percentage
Cu-Nafion	$C\|_{Cu-Nafion}$	4.26%
Cu-H_2O (capillary condensed)	$C(RH = 100)\|_{Cu-H_2O}$	7.94%
Cu-KOH solution	$C\|_{Cu-KOH}$	87.8%

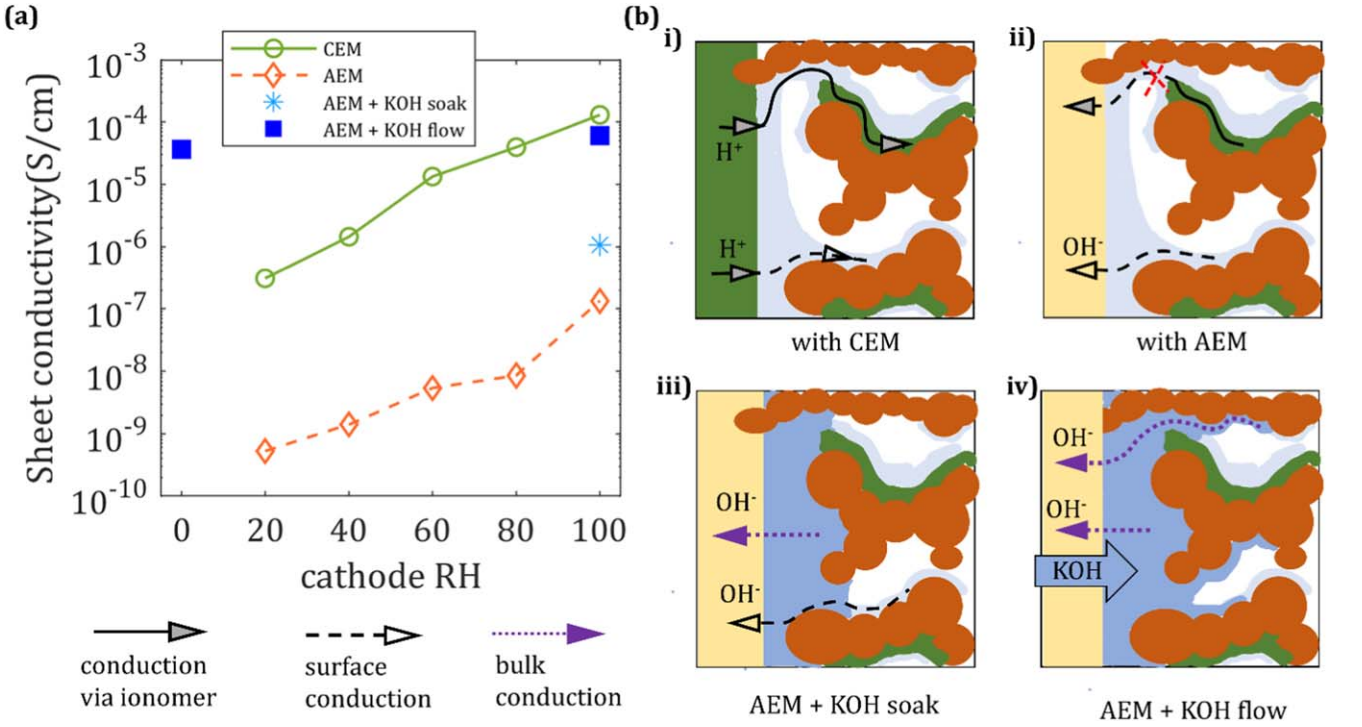

Figure 4. Ionic conductivity inside cathode vs RH for different experimental setups. The *Y* axis is plotted in logarithmic scale. Different types of conduction mechanisms are shown with different arrow styles. With KOH flow, conductivity was much higher.

H^+ conduction through the Nafion channel can also occur in principle, however, as OH^- conducts through the membrane, local conservation of charge dictates that a bipolar junction would appear somewhere inside the electrode where water dissociation must occur. The order of magnitude difference in the conductivities in these two configurations (CEM and AEM) indicate that the secondary ion-conduction mechanism (via surface conduction or) is much weaker. From Eq. 4, we can put $\kappa(RH = 100)|_{OH^-,Cu-H_2O} = 4.54 \times 10^{-7}$ S cm^{-1}.

Now, we make a simple assumption that at any hydration level, the ratio of surface conductivity of H^+ and OH^- is approximately equal to the ratio of their bulk conductivities at infinite dilution. The rationale behind this assumption is the following: surface ionic conductivity is influenced by local electric fields that arises due to the charge on Cu (potentiostatic charging). Assuming similar magnitudes of charging in these two setups (AEM and CEM), it is reasonable to expect that the conductivities would follow similar ratio as in dilute solution. Molar conductivities (λ) of H^+ and OH^- at infinite dilution are 349.65 $\times$ 10^{-4} m^2 S mol^{-1} and 198 $\times$ 10^{-4} m^2 S mol^{-1} respectively.[36] With this assumption, we have:

$$\kappa(RH)|_{H^+,Cu-H_2O} = \kappa(RH)|_{OH^-,Cu-H_2O} \times \frac{\Lambda_{H^+}}{\Lambda_{OH^-}} \; S/cm \qquad [8]$$

Calculations from Eq. 8 were used to approximate the relative contributions of surface ionic conductivity and bulk ionic conductivity of KOH later.

Next, we explain the conductivity data with KOH soak. When the electrode was soaked in KOH (no KOH flow), the sheet conductivity was 3.59 $\times$ 10^{-6} S cm^{-1}, which is almost 10 times the conductivity found when the electrode was not soaked with KOH. As explained after Table II, while soaking, KOH made more catalyst particles electrochemically active by- 1) acting like an ion-bridge between the GDE and the membrane, and 2) penetrating inside and making more catalyst particle electrochemically active. This is explained schematically in Fig. 4(b)iii.

In the setup with KOH flow, we measured the conductivity for two RH values only- 0% RH and 95% RH. Figure 4a shows that the values are much higher than one without any flow- 1.22 $\times$ 10^{-4} S cm^{-1} for 0% RH and 2.03 $\times$ 10^{-4} S cm^{-1} for 95% RH. Even for 0% RH, the ionic conductivity is much higher in magnitude than the case Fig. 4bii. It's because the ion-conduction is dominated by the conductivity of 1 M KOH in the pore-space. The specific conductivity of 1 M KOH at 60 C is 0.3222 S cm^{-1} [37] whereas the specific conductivity of DI water is $< 5 \times 10^{-8}$ S cm^{-1}. Moreover, 1 M KOH dissociates very efficiently to K^+ and OH^- ions (base dissociation constant $K_b = 0.316$[36]). From these data, we have, $\kappa|_{KOH} \gg \kappa(RH)|_{OH^-,Cu-H_2O}$. So, bulk conduction through KOH was orders of magnitude higher than surface conduction of OH^-.

For 95% change in RH in the flowing KOH case, the ionic conductivity increased by 0.8 $\times$ 10^{-4} S cm^{-1}, which is 3 orders of magnitude higher than the surface conductivities found for the configuration in Fig. 4(b)ii ($\sim$10^{-7} S cm^{-1}). The order of magnitude is close to the one found for Fig. 4(b)i, indicating that the extra conductance is through Nafion. One possible reason is the following: KOH can penetrate those pores only where the pressure is higher than the capillary pressure. Vapor on the other hand, can penetrate any network of pores that are connected. If Nafions chains exist in those pores that are not accessible to KOH but accessible to vapor, then those chains would swell by absorbing the vapor, and form ionically connected networks with pore domains where KOH exist. Those Nafion chains would conduct K^+ ions. There is no source of H^+ in this case as it's an alkaline environment, so H^+ does not contribute to the conduction. So, in Eq. 6, we put $\kappa(RH)|_{H^+,\,Nafion} = 0$ and $\kappa(RH)|_{K^+,\,Nafion} \approx 0.8 \times 10^{-4}$ S cm^{-1}. Finally, we tabulate the ionic conductivities in alkaline environment (with AEM) in presence and absence of KOH in Table IV:

Table IV. Electrode conductivity in presence or absence of KOH.

Experimental setup	Electrode conductivity
Electrode with AEM and no KOH	4.54 $\times$ 10^{-7} S cm^{-1}
Electrode with AEM and flowing KOH	2.03 $\times$ 10^{-4} S cm^{-1}

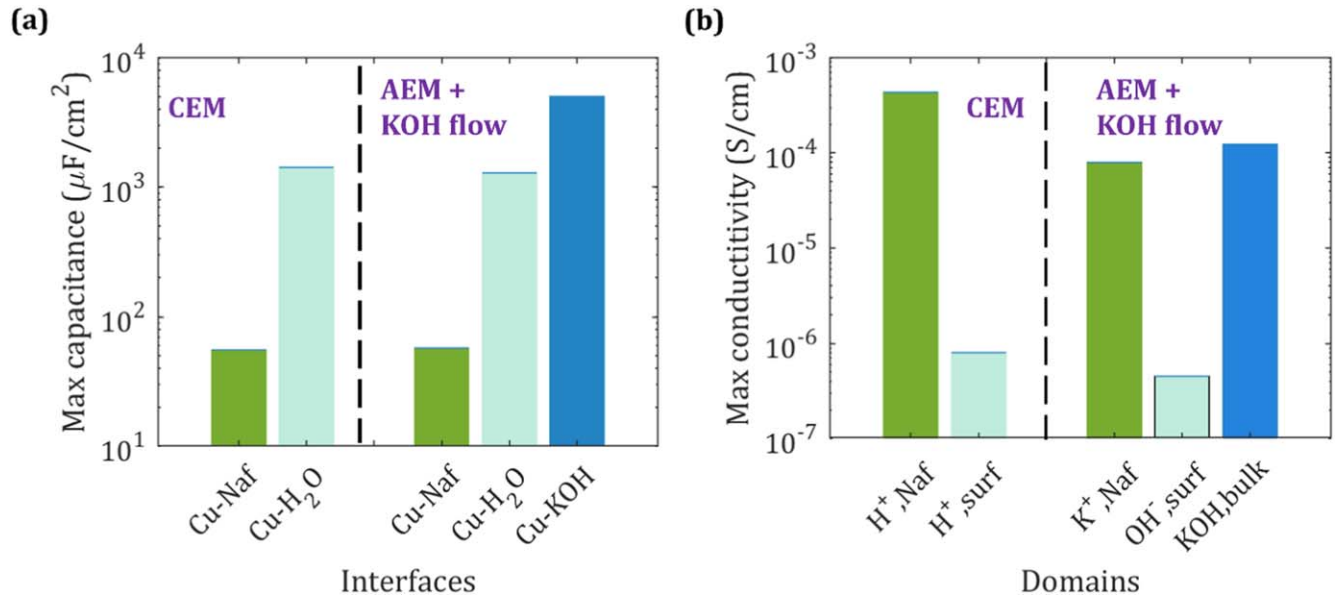

Figure 5. Overall morphological feature of a CO_2R electrode with a CEM and an AEM (with KOH flow): (a) maximum capacitances at different interfaces, showing that catalyst utilization is maximum in presence of KOH; and (b) maximum ionic conductivities in each domain. Ion conduction occurs dominantly through Nafion or KOH, not over the Cu-surface. The Y-scale is logarithmic.

Comparing the data for AEM with and without flowing KOH, three conclusions can be drawn- 1) approximately 4.22 times more catalyst area is utilized, 2) almost 87.8% of the catalyst area is in contact with KOH, and 3) the electrode conductivity is about 2–3 orders of magnitude higher when KOH is flowing. This clearly proves that KOH improves the properties of CO_2R electrodes with low amount of Nafion as the binder material. We summarize the important data, both capacitances and ionic conductivities in different domains Fig. 5:

We calculate the porosity of the electrode in the following way: volume of the electrode $V_{electrode} = 25\ cm^2 \times 16.9\ \mu m$ (SM S5). The Cu mass loading $M_{Cu} = 2.66\ mg\ cm^{-2}$ (from XRF). The density of Cu $\rho_{Cu} = 8.96\ gm\ cm^{-3}$ at 300 K.[36] So, the volume occupied by Cu inside the electrode $V_{Cu} = 6.696 \times 10^9\ \mu m^3$. Thus, the volume fraction of Cu $\varepsilon_{Cu} = V_{Cu}/V_{electrode} = 0.16$. The specific gravity of D2020 ionomer used for the Cu GDE = 1.02 (spec sheet). Following similar argument, the ionomer volume fraction $\varepsilon_{ionomer} = 0.09$. So, the void fraction inside the Cu GDE was $\varepsilon_{void} = 1 - \varepsilon_{Cu} - \varepsilon_{ionomer} = 0.75$.

Estimating the porosity in this way, we can calculate the tortuosity in the ionomer and pore-space distribution. The details of this calculation are provided in SM S4. We avoided providing the details here as this is not directly relevant to the theme of this paper, but a side issue. Moreover, this is an electrode specific property, i.e., it depends on the electrode composition. From the calculations, the ionomer tortuosity in the maximum hydration (100% RH) was 19.2. In 20% RH, it was 347. When RH increases, Nafion absorbs water, swells, and form a better-connected network. This is why the tortuosity decreases with increasing RH. The high tortuosity, even at 100% RH, indicates that ionomer distribution inside the electrode is highly fragmented. This may imply a strong interaction between Cu and Nafion ionomer, which may decrease if a catalyst support is used. In addition to being a binder and making the local environment alkaline, Nafion seems to interact with the Cu particles strongly.

It has already been shown that KOH improves OER kinetics, catalyst utilization inside the anode, and membrane conductivity in an AEM water electrolyzer.[5] It also promotes CO_2RR over HER.[6] This study improves the understanding of how anolyte KOH effects the CO_2R electrode properties in zero-gap CO_2 electrolyzers. Historically, commercially available anion exchange binders have not been chemically and mechanically as stable as the cation exchange binders like Nafion.[38–40] It is also difficult to disperse them inside fuel cell electrodes. Because of these reasons, Nafion has often been used as the binder of choice even for AEM fuel cells. It was also postulated that the hydrophobic nature of Nafion's backbone also helps CO_2 transport and maximizes the catalyst active area.[14] Although one needs to decouple chemistry and physical properties when swapping ionomeric binder material for CO_2R devices, our study insidcates that catalyst utilization and ionic conductivity inside the CO_2R electrode will be much higher if flowing KOH is used in the system. To the best of our knowledge, there is only one work where the authors claimed to operate a CO_2 electrolyzer with an in-house AEM and anion-exchange binder that resulted in high FE of CO_2RR products, low overpotential, and 100 h of stability.[41] However, little is known about the electrocatalyst/ionomer interactions for such a system which may depend just as much on the processing of the materials as well as their inherent properties. Unless alternate pathways are pursued to enhance cathode catalyst utilization (ionic accessibility) at low RH, anolyte flow seems to be essential for CO_2 electrolyzers to increase catalyst utilization, ionic conductivity, and perhaps product selectivity inside the CO_2R electrodes.

Experimental

Materials.—50 wt% Pt/C catalyst (TEC10E50E, TKK Lot #1020-A971 with 46.7% actual Pt wt%) from TANAKA Precious Metals were used to fabricate the anode GDE. Cu nanoparticles (40 nm) from U.S. Research Nanomaterials was used to fabricate the cathode GDE. 27.5 μm thick Nafion XL (Ion-Power Inc.) was used as the CEM and 25 μm thick Aemion + (AF2-CLE8–25-X) (Ionomr Innovations) was used as the AEM. Both membranes had reinforcement layers. The cell hardware components were the same as reported in previous publications from our group.[42] Nickel and titanium were used as the anode and cathode flow field materials respectively. For the KOH chamber, chemically inert polyeherimide (PEI) film (McMaster Carr) were used.

KOH pellets (>85.0% Emsure from Sigma Aldrich) were used to make the KOH solution. ASTM I quality DI water (Milli-Q) was used for all purposes.

Electrode fabrication.—The anode catalyst ink was prepared following established protocols [43,44] by mixing 50 wt% Pt supported on high surface area carbon catalyst powder, 20 wt% D2020 Nafion dispersion, n-propyl alcohol, and water. The nPA to water ratio was

kept 2:3 as this dispersion showed the optimal catalyst-ionomer interaction.[45] For application with CEM (Fig. 1a), the ionomer loading was 30% by weight (~0.9 ionomer to carbon ratio). For application with AEM (Figs. 1b and 1c), 3 wt% ionomer loading was used (~0.2 ionomer to carbon). The ink was horn-sonicated for 10 s. Then it was ultrasonicated for 45 min in an ice-water bath. Then the ink was sprayed on SGL39BB gas diffusion layer (GDL) with 5 wt% PTFE loading on the microporous layer (MPL) side by the Sono-Tek spray station with a 25 kHz accumist nozzle. The final Pt loading was 0.22 ± 0.013 mg cm^{-2} as determined by X-ray fluorescence (XRF) (Fisher XDV-SDD). The spray area was approximately 50 cm^2.

The cathode catalyst ink was prepared by mixing 3.0 g isopropanol and 3.1 g water in a 20 ml glass vial and then adding 0.9 g Nafion D2020. While stirring this mixture with a magnetic stir bar, 3 g of Cu nanoparticles (U.S. Research Nanomaterials, 40 nm) were added. After dispersion of the particles in the solvent (1–5 min), the stir bar was removed, and 55 g of 5 mm zirconium oxide beads (Glen Mills) were added. The vial was taped and placed on a roller at 80 rpm for 19–24 h. After milling, the ink was rod-coated onto Sigracet 39 BB by placing a ~5 × 8 cm piece of gas diffusion media onto an Automatic Film Applicator, depositing 2–3 ml of ink and rolling at 55 mm s^{-1} at room temperature with a number 25 rod. The electrodes were then transferred to an 80 °C oven for 5–10 min to dry.

The AEM was soaked in 1 M KOH overnight to exchange the counter ions (I^- and Cl^-) and to delaminate it from the backing layer.

Cell assembly.—The GDEs in Figs. 1a and 1b were assembled in zero-gap configuration with two 228.6 μm thick PTFE gaskets to achieve 20% compression on both anode and cathode. 25 cm^2 cell area was cut from the 50 cm^2 sprayed area. For one setup, the Cu GDE was soaked in 1 M KOH in a container separate from the one where the AEMs were soaked.

The configuration shown in Fig. 1c was achieved in a different way. In this configuration, two electrolyte holes were drilled in the anode flow field made of nickel. Two AEMs were used, one on the anode side and the other on the cathode, to separate them from the KOH chamber. The KOH chamber was made by putting 10 PEI films (McMaster Carr), each 0.005' thick, between the anode side and the cathode side membrane. The electrolyte KOH entered and exited the chamber through the anode flow-field holes. There was no hole for KOH to go through and wet the Cu GDE. The only way KOH could reach the Cu GDE is by crossing through the AEM. This setup mimicked the condition in a zero-gap CO_2 electrolyzer. The cell design is very similar to that used in the study from our group where a CO_2 electrolyzer cell with a catholyte container was designed for high formate production.[42] The difference in our case was that we created a chamber to circulate an anolyte rather than a catholyte.

Electrochemical Diagnostics.—*Gas flow conditions:* The cells that had no KOH in them were subjected to the same electrochemical protocol. After assembly, they were connected with a Hydrogex fuel cell test station. All the experiments were done at 60 C. Nafion is known to be stable at 80 C but not the AEMs. The official documentation of Aemion membranes recommend using a temperature below 80 C. At 60 C, the lowest RH we could go to is 20%. After setting the temperature and the initial cathode RH (20%), the gas flows (100% H_2 at anode N_2 at cathode). The cathode RH was changed from the lowest (20%) to the highest (100%). The anode RH was kept constant 100% because at very low RH, the ionic conductivity in the anode decreased significantly. A significant overpotential developed at the anode as a result.

The gas backpressure was kept 100 kPa and the flow rate was 0.2 SLPM. The total backpressure was adjusted to maintain the 100 kPa gas pressure. At 60 C, the saturated vapor pressure of water is 20 kPa So, for certain cathode RH, total gas backpressure = 100 kPa + RH/100*20 kPa. The anode backpressure was kept constant at 120 kPa. At low cathode RH, some water vapor may have crossed over to the cathode due to this pressure differential. However, stable EIS curves were obtained for each RH.

For the setup where the electrode was soaked in KOH, a slightly different protocol was used. After assembly, the cathode RH was set to 100% and conditioned. If the RH was low, then KOH would be purged out easily due to evaporation. We performed only one experiment in this condition as KOH gets purged slowly from the system.

For the setup with KOH flow (Fig. 1c), a different protocol was used. This test was done in a custom-built electrochemical test station that is equipped with a strong chemical exhaust hood. The reasons to use a different test station are- 1) when both H_2 is flowing in the anode and the KOH is being circulated, some H_2 comes out in the KOH bottle. Some KOH drops also come out through the H_2 outlets. They got mixed. So, we needed a strong hood for ventilation. 2) The KOH could go inside the fuel cell test controllers and damage the sensors. Because of the design of CO_2 test stations, we could not pressurize the H_2 gas. So, the gases (both H_2 and N_2) were not pressurized. Lower gas flow rate (0.2 SLPM) was used. KOH was circulated at 20 ml min^{-1} using an electrolyte pump. The RH control was also different from that in the fuel cell test station. At that low flow rates, we could only use very low RH (0%) or very high RH (95% or above). So, the measurements were done at 2 RH values. We could not increase the gas flow rates because of three reasons- 1) it tore the membranes due to the increased pressures, and 2) it flushed out KOH quicker than it could be refilled creating a void in the KOH container, 3) high gas flow rates created turbulence in the KOH chamber that made the EIS data noisy.

Conditioning: The electrode was conditioned in the OCV condition with H_2/N_2 gas feed (flow rate and backpressure as mentioned above) for 1 h at each RH. When a CEM was used, the initial OCV was around 260 mV and later dropped to 150 mV. The dissolution potential for Cu is ~182 mV vs standard hydrogen electrode (SHE) for pH < 5.[46] Assuming the local pH at the anode to be ~2,[47] the potential on Cu electrode was 260–59*2 = 142 mV vs SHE. So, the OCV condition was most likely a safe potential even in presence of internal currents. With just an AEM (no KOH), the initial OCV was found to be around 300 mV. This is expected as the anode potential shifted to a more negative value with respect to an SHE with increasing pH.

The setup with KOH flow (Fig. 1c) was conditioned in a similar way. KOH flow was started as soon as the cell was assembled. It was done to prevent membrane drying. Then the temperature was set, and the gas flow was initiated. Then the system was left to equilibrate for 30 min before any EIS experiments were performed. The initial EIS was about 550 mV which, after equilibration, went down to 450 mV. The KOH also crossed over to Pt/C and increased the internal pH. So, the anode was effectively at a lower potential (vs SHE) than the setup with just an AEM but no KOH flow. Due to KOH, the Cu particles might have been slightly oxidized.

EIS protocol: Potentiostatic EIS was performed at 100 mV cell voltage with 20 mV root mean square AC perturbation for all setups. The potential was chosen for the following reasons- 1) The potential must be >0 to minimize the effect of HER, 2) the potential must be less than the dissolution potential, 3) it should be close to potential of zero charge for Cu to avoid effects of physisorption or chemisorption (surface oxides or complexes). Pourbaix diagram for Cu indicates that in acidic environment, planar Cu dissolves at ~182 mV vs SHE at 25 C. The average Cu catalyst particles size was 40 nm, which reduces the dissolution potential due to the Gibbs-Thomson effect[48] by:

$$\mu(r) = \mu(r = \infty) - \frac{2\gamma_{Cu} V_{Cu}}{r} \quad [9]$$

Where μ(r) and μ(r = ∞) are the chemical potentials of Cu in particle form (of radius "r") planar form respectively. γ_{Cu} is the

surface free energy of Cu and V_{Cu} is its molar volume. $\gamma_{Cu} = 1.756$ J m^{-2} at 358 K and $V_{Cu} = 7.11$ cm^3 mol^{-1}.[49] From here, one can calculate the dissolution potential for the particle to be:

$$E_{diss}(r) = E_{diss}(r = \infty) - \frac{\Delta\mu}{zF} = 182 - 6.48\,mV = 175.52\,mV$$

Here, z = 1. The correction due to Gibbs-Thompson effect for 40 nm particles is negligible. This effect is stronger for smaller nanoparticles, for example, in Pt/C electrodes, as the Pt particles are ~ 3 nm in size.

The potential of zero charge (PZC) for polycrystalline Cu is approximately −640 mV vs SHE around pH 3.[50] Assuming the local pH at anode to be ~2,[47] the potential at the anode was ~0 − 59*2 = −118 mV vs SHE. So, in order to apply a potential close to PZC, we had to apply negative cell potential. But that would produce HER. So, there was no way to choose a potential close to PZC and avoid HER at the same time. So, we neglected the criterion number 3. Due to this problem, the surface charge on Cu was most likely different in different setups. For example, with CEM, the surface charge was highly negative. With AEM and KOH flow, the surface charge was less negative (as the anode potential was more negative). Ideally, different capacitance curves should be considered at similar charging conditions, as according to the Gouy-Chapman-Stern theory, the differential double layer capacitance (C_{DL}) depending on the surface charge. Sheet capacitance is the product of C_{DL} and electrochemical active area. If C_{DL} changes in different setups, one cannot have an apple-to-apple comparison.

The frequency range was chosen from 300 kHz to 0.1 Hz. We used Gamry 3000 potentiostat (both with and without the booster). 300 kHz is the maximum frequency that the potentiostat can generate. We did not go below 0.1 Hz to avoid any low frequency apparent inductive behavior.[51,52] The "normal" data acquisition mode was chosen. 20 mV AC perturbation was chosen as it was the maximum perturbation potential which satisfied the Kramers-Kronig (KK) criterion, and hence, satisfied linearity, causality, and stability.[53] The internal Gamry code for KK test was used for this.

Micro Xray tomography (micro XCT).—The GDE catalyst layer thickness is quantified with a micro Xray computed tomography instrument (micro XCT, NSI X3000, North Star Imaging, Inc. USA.) During the characterization, the X-ray source has a voltage of 80 kV and emission current of 250 μA. The GDE sample was mounted on the rotation stage and rotated for 360 degrees during the full acquisition. 1080 projections were taken during the scan with 30 frames averaged for each projection. Details of the technique are reported elsewhere.[54]

Conclusions

Herein, an experimental method to study the properties of CO_2 reduction electrodes (like catalyst utilization, ionic accessibility etc.) without the complexities of co-electrolysis of a CO_2 electrolyzer was developed. This study showed that flowing anolyte in zero-gap CO_2R devices improves the cathode by increasing the catalyst utilization as well as the ionic conductivity. We used an unsupported Cu gas diffusion electrode with low Nafion content as the model electrode and 1 M KOH as the anolyte. We found, by comparing the electrochemical data in presence and absence of anolyte, that the electrochemically active area and ionic conductivity inside the electrode increased 4 and 447 times respectively. Liquid anolyte wetted the electrode's pore space more efficiently than the capillary condensed water vapor could. Surface ion conduction (both H^+ and OH^-) was orders of magnitude weaker than the ion-conduction inside bulk KOH. The ionomer coverage was very low (~4%) and its distribution was highly fragmented (tortuosity ~19 at maximum hydration). With the present state of commercially available ionomer binders, our study indicates that an anolyte flow is essential not only for the electrolyzer anode and the anion exchange membrane, but also for the cathode. The method developed in this study can be utilized to optimize CO_2 reduction processes targeting a variety of products.

Acknowledgments

This work was authored by Alliance for Sustainable Energy, LLC, the manager and operator of the National Renewable Energy Laboratory for the U.S. Department of Energy (DOE) under Contract No. DE-AC36–08GO28308. The techniques developed in this work were funded by the Bio Energy Technology Office. The electrodes developed in this work were fabricated with funding from Shell's New Energies Research and Technology (NERT) Dense Energy Carriers program overseen by Sumit Verma. The views expressed in the article do not necessarily represent the views of the DOE or the U.S. Government. The U.S. Government retains and the publisher, by accepting the article for publication, acknowledges that the U.S. Government retains a nonexclusive, paid-up, irrevocable, worldwide license to publish or reproduce the published form of this work, or allow others to do so, for U.S. Government purposes.

ORCID

Prantik Saha https://orcid.org/0000-0001-9417-6872
Tim Van Cleve https://orcid.org/0000-0001-7233-5844
K. C. Neyerlin https://orcid.org/0000-0002-6753-9698

References

1. P. Friedlingstein, M. O'Sullivan, M. W. Jones, R. M. Andrew, J. Hauck, A. Olsen, G. P. Peters, and S. Zaehle et al., *Earth System Science Data*, **12**, 3269 (2020).
2. Y. Hori, *Modern Aspects of Electrochemistry*, ed. C. G. Vayenas et al. (Berlin) (Springer) p. 89 (2008).
3. D. M. Weekes, D. A. Salvatore, A. Reyes, A. Huang, and C. P. Berlinguette, *Acc. Chem. Res.*, **51**, 910 (2018).
4. D. Higgins, C. Hahn, C. Xiang, T. F. Jaramillo, and A. Z. Weber, *ACS Energy Lett.*, **4**, 317 (2018).
5. J. Liu, Z. Kang, D. Li, M. Pak, S. M. Alia, C. Fujimoto, G. Bender, Y. S. Kim, and A. Z. Weber, *J. Electrochem. Soc.*, **168**, 054522 (2021).
6. C.-T. Dinh et al., *Science*, **360**, 783 (2018).
7. D. A. Henckel, M. J. Counihan, H. E. Holmes, X. Chen, U. O. Nwabara, S. Verma, J. Rodríguez-López, P. J. A. Kenis, and A. A. Gewirth, *ACS Catal.*, **11**, 255 (2021).
8. J. C. Bui, C. Kim, A. J. King, O. Romiluyi, A. Kusoglu, A. Z. Weber, and A. T. Bell, *Acc. Chem. Res.*, **55**, 484 (2022).
9. S. Nitopi et al., *Chem. Rev.*, **119**, 7610 (2019).
10. S. Verma, X. Lu, S. Ma, R. I. Masel, and P. J. A. Kenis, *Phys. Chem. Chem. Phys.*, **18**, 7075 (2016).
11. J. Resasco, L. D. Chen, E. Clark, C. Tsai, C. Hahn, T. F. Jaramillo, K. Chan, and A. T. Bell, *JACS*, **139**, 11277 (2017).
12. D. G. Wheeler, B. A. W. Mowbray, A. Reyes, F. Habibzadeh, J. He, and C. P. Berlinguette, *Energy Environ. Sci.*, **13**, 5126 (2020).
13. Q. Wang, H. Dong, H. Yu, and H. Yu, *J. Power Sources*, **279**, 1 (2015).
14. A. Ozden et al., *ACS Energy Lett.*, **5**, 2811 (2020).
15. H. Pan and C. J. Barile, *Energy Environ. Sci.*, **13**, 3567 (2020).
16. F. P. García de Arquer et al., *Science*, **367**, 661 (2020).
17. K. P. Kuhl, E. R. Cave, D. N. Abram, and T. F. Jaramillo, *Energy Environ. Sci.*, **5**, 7050 (2012).
18. A. N. Kuhn, H. Zhao, U. O. Nwabara, X. Lu, M. Liu, Y.-T. Pan, W. Zhu, P. J. A. Kenis, and H. Yang, *Adv. Funct. Mater.*, **31**, 2101668 (2021).
19. S. Faucher et al., *J. Phys. Chem. C*, **123**, 21309 (2019).
20. Y. Gao, J. Huang, Y. Liu, and S. Chen, *Current Opinion in Electrochemistry*, **13**, 107 (2019).
21. P. Saha, C. Nam, M. A. Hickner, and I. V. Zenyuk, *J. Phys. Chem. C*, **123**, 19493 (2019).
22. P. Saha and I. V. Zenyuk, *J. Electrochem. Soc.*, **168**, 46511 (2021).
23. P. Saha and I. V. Zenyuk, *J. Phys. Chem. C*, **125**, 19706 (2021).
24. J. McBreen, *J. Electrochem. Soc.*, **132**, 1112 (1985).
25. E. L. Thompson and D. Baker, *ECS Trans.*, **41** (2011).
26. L. Hu, M. Zhang, S. K. Babu, A. Kongkanand, and S. Litster, *ChemElectroChem*, **6**, 2659 (2019).
27. H. Iden and A. Ohma, *J. Electroanal. Chem.*, **693**, 34 (2013).
28. H.-J. Butt, K. Graf, and M. Kappl, *Phys. Chem. Interfaces* (New York)(John Wiley & Sons) (2003).
29. M. Eikerling and A. A. Kornyshev, *J. Electroanal. Chem.*, **475**, 107 (1999).
30. R. Makharia, M. F. Mathias, and D. R. Baker, *J. Electrochem. Soc.*, **152**, A970 (2005).
31. Y. Liu, M. Murphy, D. Baker, W. Gu, C. Ji, J. Jorne, and H. A. Gasteiger, *ECS Trans.*, **11**, 473 (2007).
32. S. Shi, A. Z. Weber, and A. Kusoglu, *J. Membr. Sci.*, **516**, 123 (2016).
33. Y. Zheng et al., *Macromolecules*, **51**, 3264 (2018).
34. S. A. Mauger, J. R. Pfeilsticker, M. Wang, S. Medina, A. C. Yang-Neyerlin, K. C. Neyerlin, C. Stetson, S. Pylypenko, and M. Ulsh, *J. Power Sources*, **450**, 227581 (2020).

35. Y. Sone, P. Ekdunge, and D. Simonsson, *J. Electrochem. Soc.*, **143**, 1254 (1996).
36. W. M. Haynes, D. R. Lide, and T. J. Bruno, *Handbook of Chemistry and Physics* 95th ed. ed.(Boca Raton, FL)(Hoboken)(CRC Press) (2014).
37. R. J. Gilliam, J. W. Graydon, D. W. Kirk, and S. J. Thorpe, *Int. J. Hydrogen Energy*, **32**, 359 (2007).
38. D. A. Salvatore et al., *Nat. Energy*, **6**, 339 (2021).
39. R. B. Kutz, Q. Chen, H. Yang, S. D. Sajjad, Z. Liu, and I. R. Masel, *Energy Technology*, **5**, 929 (2017).
40. B. Mayerhöfer, F. D. Speck, M. Hegelheimer, M. Bierling, D. Abbas, D. McLaughlin, S. Cherevko, S. Thiele, and R. Peach, *Int. J. Hydrogen Energy*, **47**, 4304 (2022).
41. Z. Yin, H. Peng, X. Wei, H. Zhou, J. Gong, M. Huai, L. Xiao, G. Wang, J. Lu, and L. Zhuang, *Energy Environ. Sci.*, **12**, 2455 (2019).
42. Y. Chen, A. Vise, W. E. Klein, F. C. Cetinbas, D. J. Myers, W. A. Smith, W. A. Smith, W. A. Smith, T. G. Deutsch, and K. C. Neyerlin, *ACS Energy Lett.*, **5**, 1825 (2020).
43. M. Wang, J. H. Park, S. Kabir, K. C. Neyerlin, N. N. Kariuki, H. Lv, V. R. Stamenkovic, D. J. Myers, M. Ulsh, and S. A. Mauger, *ACS Appl. Energy Mater.*, **2**, 6417 (2019).
44. A. M. Park et al., *ECS Trans.*, **80**, 957 (2017).
45. T. Van Cleve et al., *ACS Appl. Mater. Interfaces*, **11**, 46953 (2019).
46. B. Beverskog and I. Puigdomenech, *J. Electrochem. Soc.*, **144**, 3476 (1997).
47. M. Umeda, K. Sayama, T. Maruta, and M. Inoue, *Ionics*, **19**, 623 (2013).
48. W. J. Plieth, *J. Phys. Chem.*, **86**, 3166 (1982).
49. W. R. Tyson and W. A. Miller, *Surf. Sci.*, **62**, 267 (1977).
50. A. Łukomska and J. Sobkowski, *J. Electroanal. Chem.*, **567**, 95 (2004).
51. S. K. Roy, M. E. Orazem, and B. Tribollet, *J. Electrochem. Soc.*, **154**, B1378 (2007).
52. B. P. Setzler and T. F. Fuller, *J. Electrochem. Soc.*, **162**, F519 (2015).
53. M. Urquidi-Macdonald, S. Real, and D. D. Macdonald, *Electrochim. Acta*, **35**, 1559 (1990).
54. L. Dunsmore, A. Uddin, H. Zhang, G. Wu, and S. Litster, *J. Power Sources*, **506**, 230188 (2021).